BIOCHEMISTRY
including biophysical chemistry & molecular biology

Article

pubs.acs.org/biochemistry

Redox Thermodynamics of High-Spin and Low-Spin Forms of Chlorite Dismutases with Diverse Subunit and Oligomeric Structures

Stefan Hofbauer,[†] Marzia Bellei,[‡] Axel Sündermann,[§] Katharina F. Pirker,[∥] Andreas Hagmüller,[⊥] Georg Mlynek,[⊥] Julius Kostan,[⊥] Holger Daims,[@] Paul G. Furtmüller,[†] Kristina Djinović-Carugo,[⊥,#] Chris Oostenbrink,[§] Gianantonio Battistuzzi,[▽] and Christian Obinger*[,†]

[†]Department of Chemistry, Division of Biochemistry, VIBT-Vienna Institute of BioTechnology, BOKU-University of Natural Resources and Life Sciences, A-1190 Vienna, Austria

[‡]Department of Life Sciences, University of Modena and Reggio Emilia, 41100 Modena, Italy

[§]Department of Material Sciences and Process Engineering, Institute of Molecular Modeling and Simulation, VIBT-Vienna Institute of BioTechnology, BOKU-University of Natural Resources and Life Sciences, A-1190 Vienna, Austria

[∥]Health and Environment Department, Environmental Resources and Technologies, AIT-Austrian Institute of Technology GmbH, A-3430 Tulln, Austria

[⊥]Department for Structural and Computational Biology, Max F. Perutz Laboratories, University of Vienna, Campus Biocenter 5, A-1030 Vienna, Austria

[@]Department of Microbial Ecology, University of Vienna, A-1090 Vienna, Austria

[#]Department of Biochemistry, Faculty of Chemistry and Chemical Technology, University of Ljubljana, Aškerčeva 5, 1000 Ljubljana, Slovenia

[▽]Department of Chemistry and Geology, University of Modena and Reggio Emilia, 41100 Modena, Italy

Supporting Information

ABSTRACT: Chlorite dismutases (Clds) are heme *b*-containing oxidoreductases that convert chlorite to chloride and dioxygen. In this work, the thermodynamics of the one-electron reduction of the ferric high-spin forms and of the six-coordinate low-spin cyanide adducts of the enzymes from *Nitrobacter winogradskyi* (NwCld) and *Candidatus* "Nitrospira defluvii" (NdCld) were determined through spectroelectrochemical experiments. These proteins belong to two phylogenetically separated lineages that differ in subunit (21.5 and 26 kDa, respectively) and oligomeric (dimeric and pentameric, respectively) structure but exhibit similar chlorite degradation activity. The $E^{\circ\prime}$ values for free and cyanide-bound proteins were determined to be −119 and −397 mV for NwCld and −113 and −404 mV for NdCld, respectively (pH 7.0, 25 °C). Variable-temperature spectroelectrochemical experiments revealed that the oxidized state of both proteins is enthalpically stabilized. Molecular dynamics simulations suggest that changes in the protein structure are negligible, whereas solvent reorganization is mainly responsible for the increase in entropy during the redox reaction. Obtained data are discussed with respect to the known structures of the two Clds and the proposed reaction mechanism.

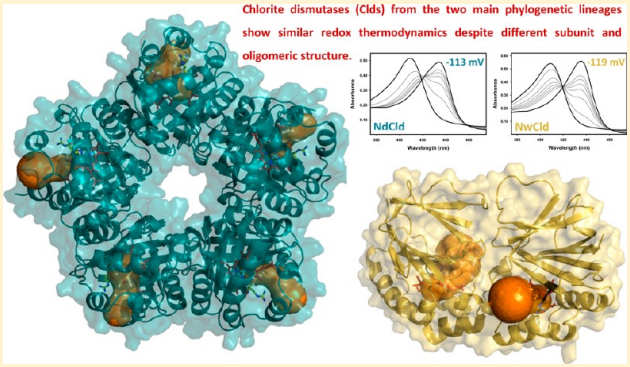

Heme proteins conduct a myriad of diverse biological functions such as O_2 transport, storage and reduction, electron transport, oxidation and oxygenation of manifold organic and inorganic compounds, hydrogen peroxide dismutation, O_2, NO, and CO sensing, etc.[1] The distinct reactivity of these oxidoreductases is determined by (i) the architecture of the active site and the substrate access channel(s), (ii) the conformation and modification of the prosthetic group, (iii) the nature of the proximal ligand of the heme iron and its mode of interaction with outer sphere ligands, (iv) the interaction of the two heme propionates with the protein, and (v) the nature and position of amino acids as well as the amount of space at the distal heme site where substrate binding and conversion take place.[1] All these factors determine the redox chemistry of the respective metalloproteins and as a consequence their (bioinorganic) reaction mechanism.[1]

Chlorite dismutases (Clds) are recently described heme *b* oxidoreductases (EC 1.13.11.49) found in prokaryotic organ-

Received: September 25, 2012
Revised: November 2, 2012
Published: November 5, 2012

   dx.doi.org/10.1021/bi3013033 | *Biochemistry* 2012, 51, 9501−9512

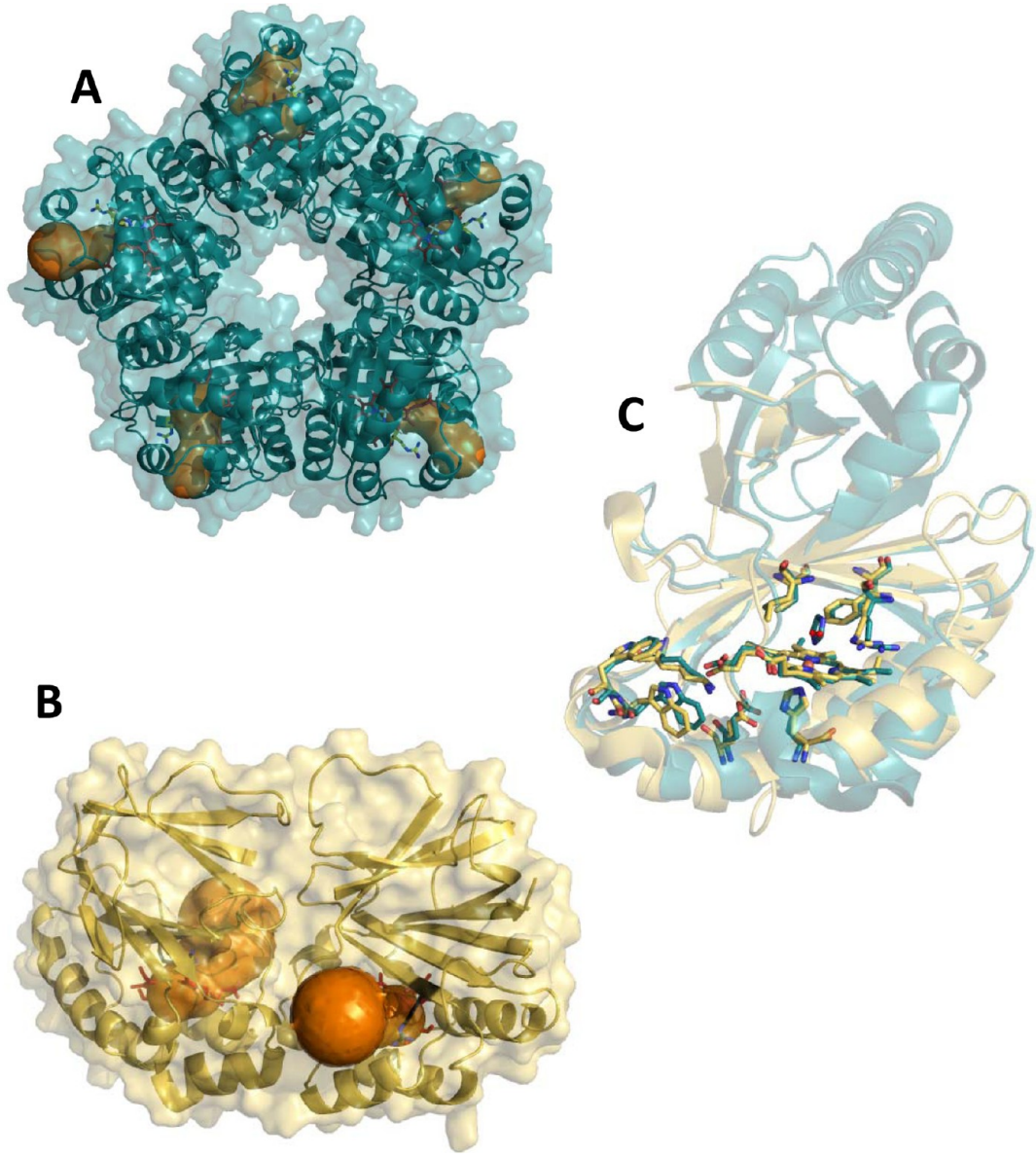

Figure 1. Overall and active site structures of chlorite dismutases from *Candidatus* "Nitrospira defluvii" (NdCld) and *N. winogradskyi* (NwCld). (A) Ribbon representation of pentameric NdCld (PDB entry 3NN1) after a 2 ns molecular dynamics (MD) simulation showing the secondary structure and semitransparent protein surface (cyan). Each subunit shows a heme *b* (red) as well as the catalytically important Arg173 of the distal heme side (yellow). Substrate channels leading to heme *b*, determined with CAVER, are colored orange. (B) Ribbon representation of dimeric NwCld (PDB entry 3QPI) after a 2 ns MD simulation showing the secondary structure and semitransparent protein surface (yellow), heme *b* (red), distal Arg127 (black), and substrate channels (orange). (C) Overlay of ribbon representations of the X-ray structures of NwCld (yellow) and NdCld (cyan). Heme cavity residues are shown as sticks. Figures were generated using PyMOL (http://www.pymol.org/).

isms. The given denomination "dismutase" is misleading because Cld converts chlorite (ClO_2^-) to chloride and dioxygen. In recent years, several X-ray structures of multimeric (di, penta, and hexa) Clds and Cld-like proteins from archaea and bacteria have been published.[2−6] Together with mechanistic studies,[7−12] these structures helped to postulate an enzymatic mechanism that includes oxidation of native ferric Cld by chlorite to an oxoiron(IV)porphyryl radical intermediate [$Por^{\bullet+}Fe(IV)=O$, Compound I] and hypochlorite, which is kept in the reaction sphere of active Clds by a fully conserved distal arginine (reaction 1).

$$PorFe(III) + [O-Cl-O]^- \rightarrow Por^{\bullet+}Fe(IV)=O\cdots[O-Cl]^- \quad (1)$$

The second redox half-reaction (reaction 2) is unique because it generates an O−O bond, a reaction found so far in biology mediated only by the water splitting manganese complex of photosystem II of oxygenic phototrophic organisms and by a yet-uncharacterized enzyme of an anaerobic methane-oxidizing bacterium.[13]

$$Por^{\bullet+}Fe(IV)=O\cdots[O-Cl]^- \rightarrow PorFe(III) + O=O + Cl^- \quad (2)$$

Reaction 1 resembles the heterolytic cleavage of hydrogen peroxide forming Compound I and water that occurs in heme peroxidases and catalases (Reaction 3).[14]

dx.doi.org/10.1021/bi3013033 | *Biochemistry* 2012, 51, 9501−9512

$$\text{PorFe(III)} + \text{H–O–O–H} \rightarrow \text{Por}^{\bullet+}\text{Fe(IV)=O} + \text{H–O–H} \quad (3)$$

Reaction 2 shows similarities with the action of some peroxidases (e.g., mammalian myeloperoxidase) that can oxidize chloride to hypochlorous acid using chloride as a two-electron donor of Compound I and releasing hypochlorite as the reaction product (Reaction 4).[15,16]

$$\text{Por}^{\bullet+}\text{Fe(IV)=O} + \text{Cl}^- \rightarrow \text{PorFe(III)} + [\text{O–Cl}]^- \quad (4)$$

Understanding differences in reaction mechanisms between related heme enzymes and the driving forces of individual redox reactions requires, besides knowledge of the structure and the catalytic amino acids in the heme cavity, information about the redox thermodynamics of the respective heme centers.[17] The reduction potential ($E^{\circ\prime}$) of the Fe(III)/Fe(II) couple not only determines the stable oxidation state of the heme proteins in their native state (i.e., the ferric state for Cld) but also reflects the hierarchy of redox properties of higher oxidation states (e.g., of the Compound I/ferric protein couple), which was demonstrated for many heme peroxidases.[17] Moreover, valuable information about the mechanism of $E^{\circ\prime}$ modulation in heme proteins can be obtained from the enthalpic ($\Delta H^{\circ\prime}_{rc}$) and entropic ($\Delta S^{\circ\prime}_{rc}$) changes of the reduction reaction, measured through variable-temperature spectroelectrochemical measurements.[17] It must be mentioned that single $E^{\circ\prime}$ values of the Fe(III)/Fe(II) couple of three Clds determined by different methods can be found in the literature (Cld from *Dechloromonas aromatica*, −23 mV;[12] Cld from *Ideonella dechloratans*, −21 mV;[18] and Cld from *Azospira oryzae*, −158 mV[3]), which differ significantly (as do the UV–vis spectra in comparison to those of NdCld and NwCld)[5,6,12,18,19] despite very similar structures of the respective heme cavities.[2−6]

This paper reports for the first time the thermodynamics of Fe(III)/Fe(II) reduction of chlorite dismutases determined spectroelectrochemically by using an OTTLE cell.[17] This allows direct comparison with related heme oxidoreductases that have been investigated by the same method. Two representatives of two phylogenetically separated lineages, namely, pentameric Cld from *Candidatus* "Nitrospira defluvii" [NdCld (Figure 1A)][5] and dimeric Cld from *Nitrobacter winogradskyi* [NwCld (Figure 1B)],[6] have been analyzed. Besides differences in oligomeric architecture, the two Clds exhibit differences in subunit structure (Figure 1C)[6] as well as in conformational and thermal stability.[19] Despite these significant disparities in overall structure and stability, the heme ligation and environment in NdCld and NwCld are almost identical to those of other published structures (Figure 1C)[2−4] of this protein family.[20,21] Moreover, NdCld and NwCld exhibit similar chlorite degradation kinetics.[5,6,19]

Here we report on (i) the $E^{\circ\prime}$ values of the Fe(III)/Fe(II) couple in the ferric high-spin native forms and of the six-coordinate low-spin cyanide adducts of NdCld and NwCld, (ii) the enthalpic and entropic contribution to the reduction reaction of the high-spin forms, (iii) the calculation of the contribution of the protein and the solvent to the reduction process, and (iv) the simulation of the molecular dynamics of the ferrous and ferric forms of NwCld and NdCld. Additionally, we have compared the substrate access channel dimensions and probed the kinetics of cyanide binding and dissociation by stopped-flow spectroscopy. The findings are discussed with respect to the known structures of NdCld[5] and NwCld[6] and the proposed reaction mechanism of Cld (reactions 1 and 2) in comparison with those of related heme enzymes.

MATERIALS AND METHODS

Cloning, expression, and purification of wild-type NdCld and NwCld were described previously.[5,6,19] All chemicals were reagent grade.

Spectroelectrochemistry. All experiments were conducted in a homemade OTTLE (optical transparent thin-layer spectroelectrochemical) cell.[22] The three-electrode configuration consisted of a gold minigrid working electrode (Buckbee-Mears, Chicago, IL), a homemade Ag/AgCl/KCl_{sat} microreference electrode, separated from the working solution by a Vycor set, and a platinum wire as the counter electrode.[22] The reference electrode was calibrated against a saturated calomel (HgCl) electrode before each set of measurements. All potentials are referenced to the SHE (standard hydrogen electrode, 242 mV).

Potentials were applied across the OTTLE cell with an Amel model 2053 potentiostat/galvanostat. A constant temperature was maintained by a circulating water bath, and the OTTLE cell temperature was monitored with a Cu-costan microthermocouple. UV–vis spectra were recorded using a Varian Cary C50 spectrophotometer. The OTTLE cell was flushed with argon gas to establish an oxygen-free environment in the cell.[22]

Variable-temperature experiments were performed using a nonisothermal cell configuration.[22] The temperature of the reference electrode and the counter electrode was kept constant, whereas that of the working electrode was varied.[22] Parametrization of enthalpic and entropic components was possible via calculation of $\Delta S'^{\circ}_{rc}$ from the slope of the plot of E'° versus temperature; $\Delta H^{\circ\prime}_{rc}$ could be obtained from the Gibbs–Helmholtz equation, thus from the slope of the plot $E^{\circ\prime}/T$ versus $1/T$.[22] Experiments with NwCld and NdCld were conducted over a temperature range from 15 to 35 °C using 650 μL samples containing 6 μM NdCld and 5 μM NwCld in 150 mM phosphate buffer (pH 7.0) and 100 mM NaCl, in the presence of various mediators: methyl viologen, lumiflavine 3-acetate, methylene blue, phenazine methosulfate, and indigo. The concentration of each mediator in the cell was 4.6 μM, except for that of methyl viologen (230 μM). Nernst plots consisted of at least five points and were invariably linear with a slope consistent with a one-electron reduction process.

The experiments for the determination of the $E^{\circ\prime}$ of the cyanide adducts of NdCld and NwCld were conducted at 25 °C using 650 μL samples containing 3 μM NdCld and 4 μM NwCld in 150 mM phosphate buffer (pH 7.0) with 100 mM NaCl and 50 mM cyanide, in the presence of the same mediator set as described above.

EPR Spectroscopy. For electron paramagnetic resonance (EPR) measurements, 200 μM NdCld and 240 μM wild-type NwCld were prepared in 50 mM phosphate buffer (pH 7.0). Solutions (100 μL) were transferred in Wilmad quartz tubes (3 mm inside diameter) under an inert nitrogen atmosphere in a glovebox.

Measurements were taken at 10 K on a Bruker EMXplus continuous wave (cw) spectrometer, operating at X-band (9 GHz) frequencies, equipped with a 4122SHQE resonator and an Oxford Instruments ESR900 cryostat. EPR spectra were recorded under nonsaturating conditions using a 0.2 mW microwave power, a 100 kHz modulation frequency, a 1 mT modulation amplitude, and a 21 ms conversion time and time constant. Saturation studies confirmed the presence of the

dx.doi.org/10.1021/bi3013033 | *Biochemistry* 2012, 51, 9501−9512

individual Fe(III) species. Simulations of high-spin and low-spin Fe(III) forms were conducted using EasySpin.[23]

Transient-State Kinetics. The experiments were conducted with a stopped-flow apparatus (model SX-18MV, Applied Photophysics) equipped for both conventional and sequential measurements. The optical quartz cell with a path length of 10 mm had a volume of 20 μL. The fastest time for mixing two solutions and recording the first data point was 1.3 ms. All measurements were performed at 25 °C. For the cyanide binding studies with ferric NwCld, the conventional stopped-flow mode was used and the increase in absorbance at 420 nm was monitored. In a typical experiment, one syringe contained 2 μM NwCld in 50 mM phosphate buffer (pH 7.0) and the second syringe contained an at least 5-fold excess of cyanide in the same buffer. A minimum of three measurements were performed for each ligand concentration. The apparent second-order rate constants, k_{on}, were obtained from the slope of a plot of k_{obs} versus cyanide concentration. Additionally, the binding of cyanide to NwCld was also investigated using the diode array detector (Applied Photophysics), which allowed the synthesis of artificial sets of time-dependent spectra as well as spectral analysis of enzyme intermediates.

Molecular Dynamics Simulations. Molecular dynamics simulations of NwCld (PDB entry 3QPI) and NdCld (PDB entry 3NN1) with a reduced and oxidized heme *b* were performed using the GROMOS11 molecular simulation package[24] and GROMOS force field 54A7.[25] The proteins were solvated in periodic rectangular simulation boxes containing the simple point charge water model[26] with a minimal solute−wall distance of 0.8 nm. Chloride and sodium counterions were added to create an overall neutral system at pH 7. The systems were gradually heated to 300 K with 60 K increases in temperature every 20 ps and equilibrated at a constant pressure for 100 ps.

Simulations were subsequently performed for 2 ns, using a step size of 2 fs. Coordinates were written out every 0.5 ps. The temperature and pressure were kept constant at 300 K and 1 atm, respectively. This was achieved through weak coupling with a relaxation time of 0.1 ps for the temperature and 0.5 ps for the pressure.[27] The isothermal compressibility was set to 4.575×10^{-4} (kJ mol^{-1} nm^{-3})$^{-1}$. Bond lengths were constrained to their optimal values with a relative geometric accuracy of 10^{-4} using the SHAKE algorithm.[28] The nonbonded interactions were calculated using a twin-range cutoff,[29] and a molecular pairlist, with a short-range cutoff of 0.8 nm and a long-range cutoff of 1.4 nm. A reaction-field contribution[30] was added to the electrostatic interactions and forces to account for a homogeneous medium outside the cutoff using a dielectric permittivity of 61.[31]

To analyze the amount and behavior of the water molecules in the binding pocket and substrate channels, the radial distribution function was calculated using GROMOS++ package for the analysis of biomolecular simulation trajectories.[32] The radial distribution function is defined here as the probability of finding a particle at a given distance relative to the same probability for a homogeneous distribution of the particles.

Substrate Channel Calculation. CAVER[33] was used to detect tunnels and therefore putative substrate channels of NwCld and NdCld (PDB entries 3QPI and 3NN1, respectively). For calculation of the length of the channels, the heme iron was set as the starting point.

RESULTS

Despite significant differences in oligomeric and subunit structure and stability,[5,6,19] the overall chlorite dismutase activities of NdCld and NwCld (polarographic measurement of the initial rate of O_2 release at 25 °C and pH 7.0) are similar. For NdCld, K_M, k_{cat}, and k_{cat}/K_M were determined to be 58 μM, 35 s^{-1}, and 6.0×10^5 M^{-1} s^{-1}, respectively, whereas for NwCld, the corresponding values were 90 μM, 190 s^{-1}, and 2.1×10^6 M^{-1} s^{-1}, respectively (Table 1).

Table 1. (A) Steady-State Kinetic Parameters for Chlorite Degradation Measured Polarographically as Dioxygen Evolution Mediated by NdCld[5] and NwCld[6] and (B) Pre-Steady-State Kinetic Parameters for the Binding of Cyanide to NdCld[5] and NwCld (this study)

	NdCld	NwCld
	(A)	
K_M (μM)	58 ± 9	90 ± 12
k_{cat} (s^{-1})	35 ± 5	190 ± 14
k_{cat}/K_M (M^{-1} s^{-1})	6.0×10^5	2.1×10^6
	(B)	
k_{on} (M^{-1} s^{-1})	2.6×10^6	1.0×10^6
k_{off} (s^{-1})	9.3	2.4
K_D (μM)	3.6	2.4

The spectroscopic properties of ferric wild-type NdCld and NwCld are indicative of predominant five-coordinate high-spin heme *b*. In detail, recombinant ferric high-spin NdCld ($S = {}^5/_2$) has its Soret maximum at 408 nm, a prominent Q-band at 533 nm (shoulder at 568 nm), and a charge-transfer (CT) band at 640 nm (Figure 2A). The corresponding maxima for recombinant ferric NwCld are at 405, 506, 543, and 640 nm, respectively (Figure 2A). It is important to note that so far published spectra of the ferric form of Clds from other sources show a rather broad Soret band at extraordinary peak maxima around 392 nm,[10,11,18] which is 12−15 nm blue-shifted compared to those of NdCld and NwCld (despite the high degree of similarity in heme cavity architecture).

The cw EPR spectrum of NdCld shows the presence of two rhombically distorted high-spin forms (Figure 2B), arising from the transition of $m_s = \pm {}^1/_2$ of an $S = {}^5/_2$ system. The rhombicity (determined by the zero-field interaction parameters *D* and *E*) of the two high-spin spectra differs slightly, leading to one broader and one narrower signal in the low-field part of the EPR spectrum (Table 1 of the Supporting Information). Additionally, spectral simulation (Table 1 of the Supporting Information) suggests the occurrence of two low-spin heme species. Comparable high-spin spectra were described previously for chlorite dismutases from other sources.[3,8,18] In contrast, the cw EPR spectrum of dimeric NwCld consists of only one dominant high-spin species with axial symmetry in addition to one minor low-spin Fe(III) form (Figure 2B). This indicates a higher symmetry around the heme cavity and two comparable coordination structures in the two subunits, whereas the different EPR spectra in the homopentamer NdCld lead to the assumption that the structural environment of the heme pocket within the subunits of the pentamer varies by distortion in the *x*−*y* plane.

Figure 3A depicts a representative family of spectra of ferric NdCld at different applied potentials in the OTTLE cell. The pentameric metalloprotein is directly reduced to its ferrous form with absorption maxima at 435 and 556 nm with a clear

dx.doi.org/10.1021/bi3013033 | Biochemistry 2012, 51, 9501−9512

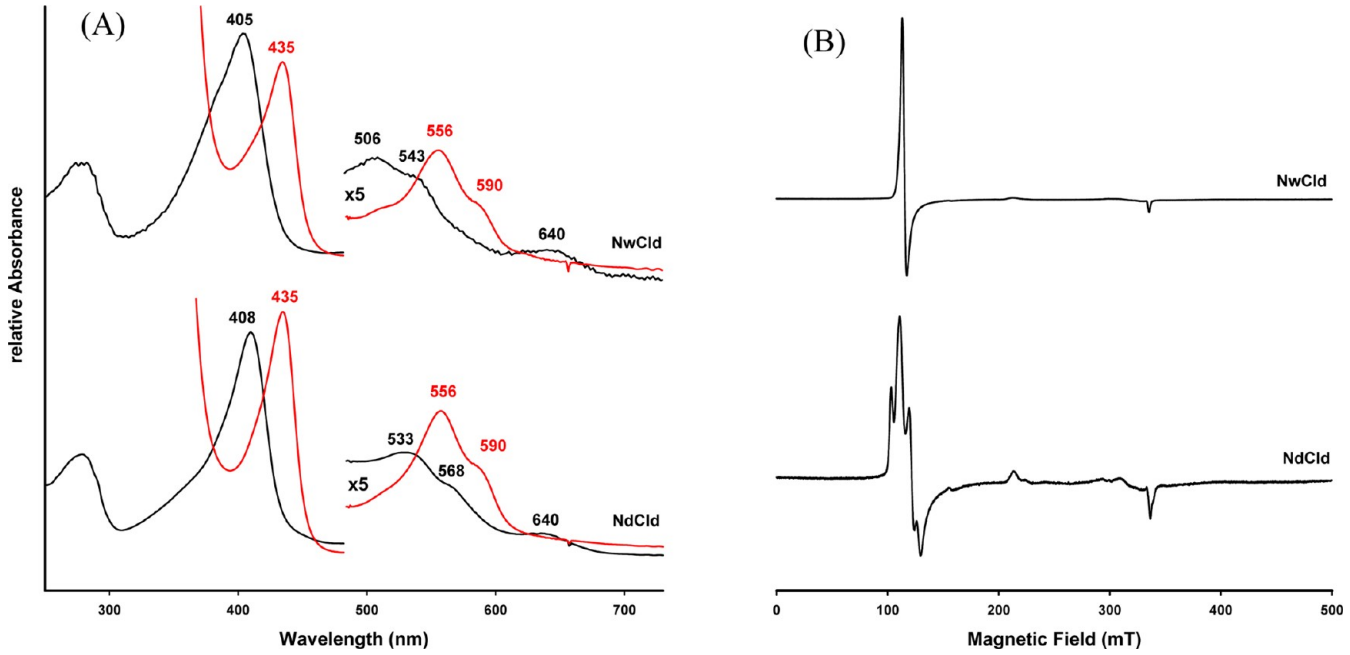

Figure 2. UV−vis and continuous wave electron paramagnetic resonance spectra of chlorite dismutases from *Candidatus* "Nitrospira defluvii" (NdCld) and *N. winogradskyi* (NwCld). (A) UV−vis spectra of NwCld and NdCld at pH 7.0. Spectra of the oxidized and reduced proteins are colored black and red, respectively. Enzymes were reduced with 10 mM sodium dithionite from a freshly prepared solution. (B) Continuous wave EPR spectra of NdCld and NwCld at pH 7.0 and 10 K.

isosbestic point at 420 nm. The calculated midpoint potential for the Fe(III)/Fe(II) couple, determined from the corresponding Nernst plot (inset of Figure 3A), was calculated to be −0.113 ± 0.001 V at 25 °C and pH 7.0. Similar experiments were performed with the dimeric chlorite dismutase from *N. winogradskyi*. Upon its direct conversion from Fe(III) to Fe(II), the identical ferrous spectrum was obtained (maxima at 435 and 556 nm, isosbestic point at 420 nm) and the standard reduction potential was very similar; i.e., $E^{\circ\prime}$ = −0.119 ± 0.002 V (25 °C, pH 7.0) (Figure 3B and Table 2).

To gain deeper insight into the mechanism of $E^{\circ\prime}$ modulation in chlorite dismutases from *Candidatus* "Nitrospira defluvii" and *N. winogradskyi*, the temperature dependence of the reduction potential of the high-spin forms was investigated (Figure 4). This allows parameterization of the corresponding enthalpic ($\Delta H^{\circ\prime}_{rc}$) and entropic ($\Delta S^{\circ\prime}_{rc}$) components of the Fe(III) to Fe(II) reduction reaction. For both metalloproteins, the oxidized state is enthalpically stabilized over the reduced state: NwCld (40 ± 4 kJ mol^{-1}) > NdCld (29 ± 6 kJ mol^{-1}) (Figure 4B and Table 3). Reduction of both species is entropically favored. The entropic components are positive for both chlorite dismutases: NwCld (95 ± 13 J mol^{-1} K^{-1}) > NdCld (63 ± 20 J mol^{-1} K^{-1}) (Figure 4A and Table 3). As a consequence, the resulting entropic contributions to $E^{\circ\prime}$ at 25 °C, i.e., 292 and 194 mV, respectively, partially compensate for the enthalpic stabilization of the ferric state, i.e., −413 and −305 mV, respectively (Table 3).

Upon addition of cyanide, both heme enzymes were converted to their low-spin complexes ($S = {}^1/_2$) exhibiting a red-shifted Soret maximum at 422 nm (isosbestic point at 413 nm) (Figure 5A). Ligand binding followed by stopped-flow spectroscopy at 420 nm was monophasic, and k_{obs} values could be obtained from single-exponential fits (Figure 5B). The apparent second-order rate constant for cyanide binding (k_{on}) was calculated from the slope of the linear plot of k_{obs} versus cyanide concentration (Figure 5C). The apparent dissociation rate constant, k_{off}, was determined from the intercept of the linear plots, allowing the calculation of the dissociation constant (K_D) of the cyanide complexes from k_{off}/k_{on} ratios. Both Clds exhibited similar kinetics and thermodynamics of cyanide binding with the following values: k_{on} = 2.57 × 10^6 M^{-1} s^{-1}, k_{off} = 9.3 s^{-1}, and K_D = 3.6 μM for NdCld,[4] and k_{on} = 1.0 × 10^6 M^{-1} s^{-1}, k_{off} = 2.4 s^{-1}, and K_D = 2.4 μM for NwCld (Table 1). These data clearly underline the fact that both access to and binding at the heme cavity of cyanide are very similar.

Next, we probed the effect of binding of the low-spin ligand cyanide on the redox properties of the Fe(III)/Fe(II) couple, performing redox titrations of cyanide complexes of both enzymes at different applied potentials (Figure 3C,D). The ferric cyanide complexes were directly reduced to the corresponding ferrous cyanide adducts (Soret band at 435 nm) with an isosbestic point at 430 nm. The calculated midpoint potentials determined from the corresponding Nernst plots are almost identical with values of −0.404 ± 0.005 V for NdCld and −0.397 ± 0.002 V for NwCld (25 °C, pH 7.0). The $E^{\circ\prime}$ values are similar to those of the six-coordinate low-spin cyanide adducts of other heme proteins (Table 2). However, the differences between the $E^{\circ\prime}$ values of high- and low-spin forms are sensibly higher in Clds (Table 2).

Because both the protein and the solvent contribute to enthalpic and entropic changes during the reduction of ferric Cld, it is important for the interpretation of data to know (i) the solvent accessibility of the heme center in the ferric and ferrous states and (ii) the extent of solvent reorganization and of conformational change of the protein during Fe(III) reduction. Thus, by using CAVER, we have identified and measured the dimensions of the substrate channels for each subunit of both proteins. Panels A and B of Figure 1 illustrate the substrate channels and their orientation within the oligomeric structures. Figure 1A shows that substrate channels

dx.doi.org/10.1021/bi3013033 | *Biochemistry* 2012, 51, 9501−9512

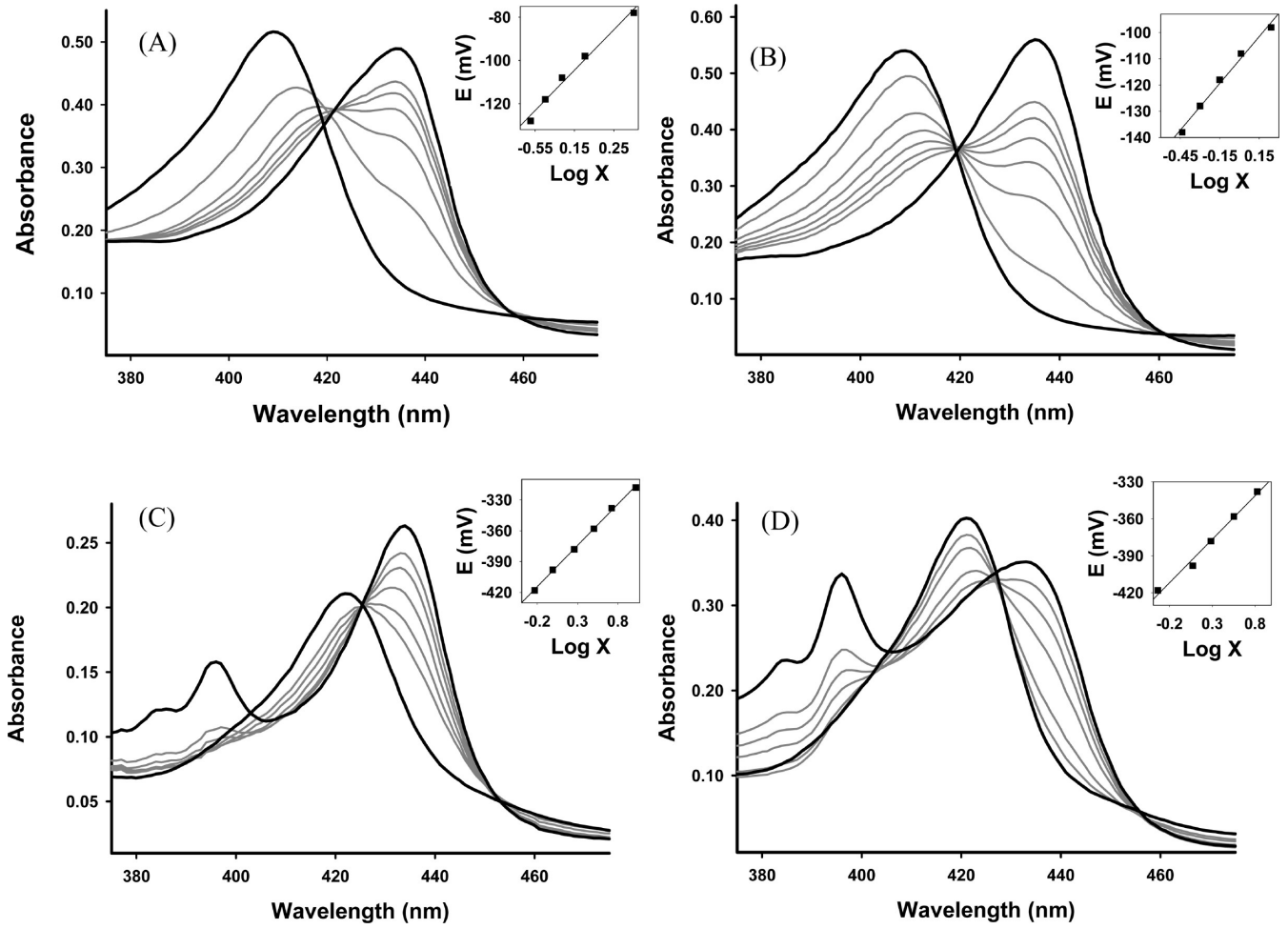

Figure 3. Spectroelectrochemical titrations of the Fe(III)/Fe(II) redox couple of the high-spin native form of chlorite dismutases from *Candidatus* "Nitrospira defluvii" (NdCld) and *N. winogradskyi* (NwCld) and their six-coordinate low-spin cyanide adducts. (A) Electronic spectra of high-spin native NdCld at various potentials at 25 °C in 150 mM phosphate buffer (pH 7.0) and 100 mM NaCl. (B) Electronic spectra of high-spin native NwCld at various potentials at 25 °C in 150 mM phosphate buffer (pH 7.0) and 100 mM NaCl. (C) Electronic spectra of the six-coordinate low-spin cyanide adduct (50 mM cyanide) of NdCld at various potentials at 25 °C in 150 mM phosphate buffer (pH 7.0) and 100 mM NaCl. (D) Electronic spectra of the six-coordinate low-spin cyanide adduct (50 mM cyanide) of NwCld at various potentials at 25 °C in 150 mM phosphate buffer (pH 7.0) and 100 mM NaCl. The insets depict the corresponding Nernst plots, where X represents $(A_{\lambda_{red}}{}^{Max} - A_{\lambda_{red}})/(A_{\lambda_{ox}}{}^{Max} - A_{\lambda_{ox}})$, where λ_{ox} = 409 nm and λ_{red} = 435 nm for high-spin NdCld, λ_{ox} = 422 nm and λ_{red} = 435 nm for the six-coordinate low-spin cyanide adduct of low-spin NdCld, λ_{ox} = 407 nm and λ_{red} = 435 nm for high-spin NwCld, and λ_{ox} = 422 nm and λ_{red} = 435 nm for the six-coordinate low-spin cyanide adduct of NwCld.

in the NdCld homopentamer are solvent-exposed on the outside of the protein and equidistant from each other. The substrate channels to heme *b* of both NwCld subunits (Figure 1B) have calculated averages for the bottleneck radius of 2.6 ± 0.05 Å, for the length of 15.7 ± 1.7 Å, and for the volume of 389 ± 27 Å^3. These values compare with the average values of the substrate channels for all five NdCld subunits (bottleneck radius of 2.8 ± 0.01 Å, length of 15.1 ± 0.9 Å, and volume of 518 ± 44 Å^3). Thus, despite the differences in overall and subunit structure, NdCld and NwCld have access channels of similar length and bottleneck radius. The observed discrepancy in volume might be explained by a more restricted channel entrance at the protein surface in NwCld (see the overlay in Figure 7A) and/or in some uncertainty in defining the position of the access channel entrance at the protein surface.

Finally, molecular dynamics simulations were performed to evaluate differences in protein structure and solvation between the ferric and ferrous state of the two Clds. Starting with the respective crystal structures,[5,6] we simulated both proteins for 2 ns in their oxidized and reduced heme states, demonstrating that the protein structures in both redox states are highly similar. For NdCld and NwCld, the backbone atom-positional root-mean-square deviations (rmsd) between the respective crystal structure and the ferric or ferrous state after a 2 ns simulation were 1.5 and 1.6 Å, and 1.3 and 1.4 Å, respectively. The calculated rmsd values for the backbone atom positions of active site residues were 1.4 and 1.4 Å, and 1.2 and 1.3 Å, respectively. It must be mentioned that both NdCld and NwCld structures as deposited in the PDB are most likely in the reduced state because of X-ray-induced radiation.[34] Additionally, no changes in the structure (including planarity) of the prosthetic group were observed (Figure 1 of the Supporting Information). These findings clearly suggest that during reduction of the ferric Clds to the ferrous state the overall protein structure and the active site are not altered.

To analyze the amount and behavior of water molecules in the binding pocket, we calculated the radial distribution function (rdf, defined here as the probability of finding a particle at a given distance relative to the same probability for a homogeneous distribution of particles). Figure 6 clearly depicts

dx.doi.org/10.1021/bi3013033 | *Biochemistry* 2012, 51, 9501−9512

Table 2. Reduction Potentials of the Fe(III)/Fe(II) Couple of High-Spin Native Forms and Six-Coordinate Low-Spin Cyanide Adducts of Chlorite Dismutases from *Candidatus* "Nitrospira defluvii" (NdCld) and *N. winogradskyi* (NwCld)[a]

	$E^{\circ\prime}$ (V)			
metalloprotein	high-spin	low-spin (cyanide adduct)	$\Delta E^{\circ\prime}$ (V)	ref
NdCld	−0.113 ± 0.001	−0.404 ± 0.005	0.291	this study
NwCld	−0.119 ± 0.002	−0.397 ± 0.002	0.278	this study
ARP	−0.183	−0.390	0.207	44
soybean peroxidase	−0.310	−0.443	0.133	45
HRP-C	−0.306	−0.430	0.124	22
cucumber basic peroxidase	−0.320	−0.412	0.092	46
MPO	0.005	−0.037	0.042	43

[a]For comparison, data from *Arthromyces ramosus* peroxidase (ARP), horseradish peroxidase isoform C (HRP-C), soybean peroxidase, cucumber basic peroxidase, and myeloperoxidase (MPO) are listed. $\Delta E^{\circ\prime}$ is the difference in the reduction potential of the Fe(III)/Fe(II) couple between high-spin and low-spin forms.

that the rdfs for the water molecules show a similar pattern for both NdCld and NwCld up to a distance of approximately 20 Å (thus including the full length of the substrate channel). In the Fe(III) state, the water dipoles are located closer to the metal ion compared to those in the Fe(II) state (see the spikes in Figure 6A,B). To investigate this further, the number of water molecules at a given distance was calculated from the rdf. In both proteins, the oxidized heme has one water molecule very close to it, and up to a distance of 7.0 Å, there are three more water molecules in the pocket than in ferrous Cld (Figure 6C). These findings reflect the solvent reorganization that occurs during the Fe(III) to Fe(II) reduction reaction (see below).

DISCUSSION

Chlorite dismutase-like proteins are found in 15 bacterial and archaeal phyla, suggesting ancient roots.[5,20] Recently, it has been demonstrated that Clds are structurally related to other protein families like dye-decolorizing heme peroxidases.[21] Indeed, when the active site of Clds and these novel peroxidases was examined, both the proximal and the distal amino acids (with the exception of the peroxidase-typical aspartate) are found at very similar positions,[21] suggesting also a comparable $E^{\circ\prime}$ value for the Fe(III)/Fe(II) couple. The two chlorite dismutases investigated in this study were selected because they belong to the two major lineages of the Cld family. Pentameric NdCld is a representative of lineage I that comprises the so-called canonical Clds all featuring very similar subunit structures and oligomerization,[2−5] whereas NwCld was the first representative of lineage II with a determined crystal structure and chlorite degradation activity (Table 1).[6] Moreover, because the two metalloproteins exhibit similar chlorite degradation kinetics and have their active site residues at very similar positions, we hypothesized that the reduction potentials might show similar values and thus could be representative for the whole Cld family.

In the native ferric state, both chlorite dismutases exhibit UV−vis and EPR spectra typical for heme *b* high-spin ($S = {}^5/_2$) enzymes. Although the subunit structure of NwCld as a typical representative of lineage II Clds is very different from that of NdCld (the primary sequence of the former is ∼30% shorter than that of the latter, with a significant deletion in the N-terminal region),[5,6] these findings clearly demonstrated that the heme ligation and environment as well as the dimension of the substrate access channel are very similar in the two enzymes (Figure 7B). Both NdCld and NwCld exhibit almost identical standard reduction potentials of the Fe(III)/Fe(II) couple of −113 and −119 mV at pH 7.0, respectively, underlining the fact that the native stable oxidation state of Cld is Fe(III).

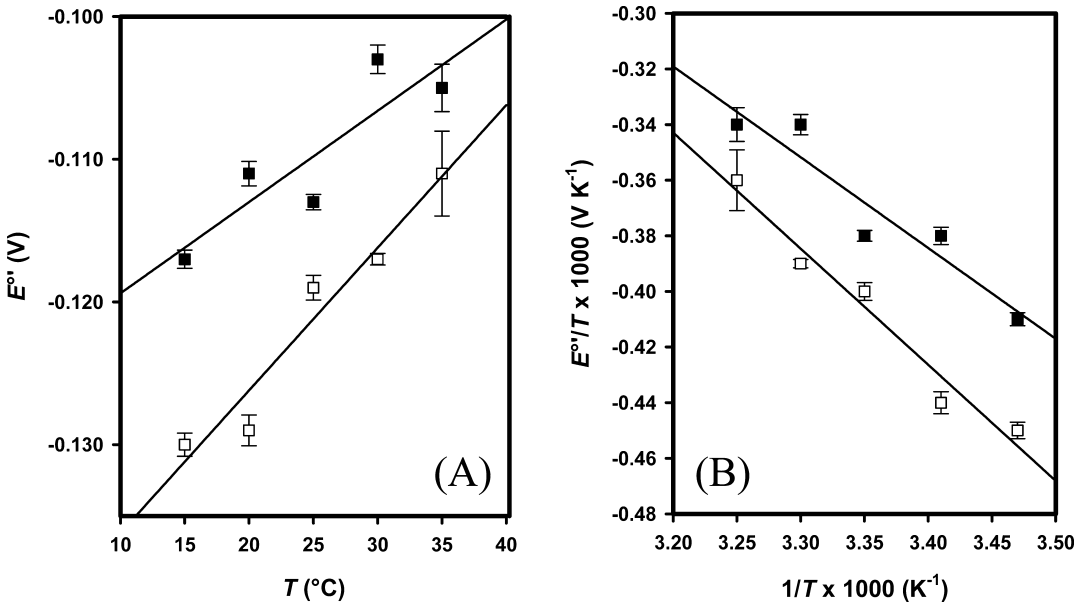

Figure 4. Redox thermodynamics of the high-spin native form of chlorite dismutases from *Candidatus* "Nitrospira defluvii" (NdCld) and *N. winogradskyi* (NwCld). (A) Temperature dependence of the reduction potential and (B) $E^{\circ\prime}/T$ vs $1/T$ plots for NdCld (■) and NwCld (□). The slopes of the plots yield the $\Delta S^{\circ\prime}_{rc}/F$ (A) and $-\Delta H^{\circ\prime}_{rc}/F$ (B) values. Solid lines are least-squares fits to the data points. All experiments were conducted in 150 mM phosphate buffer and 100 mM NaCl (pH 7.0).

dx.doi.org/10.1021/bi3013033 | *Biochemistry* 2012, 51, 9501−9512

Table 3. Thermodynamic Parameters for the Fe(III) → Fe(II) Reduction of High-Spin Native Chlorite Dismutases from *Candidatus* "Nitrospira defluvii" (NdCld) and *N. winogradskyi* (NwCld)[a]

protein	$E^{\circ\prime}$ (V)	$\Delta H^{\circ\prime}_{rc}$ (kJ mol^{-1})	$\Delta S^{\circ\prime}_{rc}$ (J mol^{-1} K^{-1})	$-\Delta H^{\circ\prime}_{rc}/F$ (V)	$T\Delta S^{\circ\prime}_{rc}/F$ (V)	$-FE^{\circ\prime}$ [$=\Delta H^{\circ\prime}_{rc(int)}$] (kJ mol^{-1})	ref
NwCld	−0.119 ± 0.005	40 ± 4	95 ± 13	−0.413 ± 0.040	0.292 ± 0.040	11.5 ± 0.1	this study
NdCld	−0.113 ± 0.005	29 ± 6	63 ± 20	−0.305 ± 0.060	0.194 ± 0.060	10.9 ± 0.1	this study
HRP-C	−0.306	91	210	−0.943	0.648	29	22
KatG	−0.226	17	−18	−0.176	−0.056	22	42
MPO	0.005	3	10	−0.031	0.031	0	43
IdCld	−0.021	–	–	–	–	–	18
AoCld	−0.023 ± 0.009	–	–	–	–	–	8
AoCld	−0.158 ± 0.009	–	–	–	–	–	3
DaCld	−0.023	–	–	–	–	–	12

[a]For comparison, the thermodynamic parameters of three heme peroxidases from different superfamilies are shown, namely, those of horseradish peroxidase isoform C (HRP-C), catalase-peroxidase (KatG) from *Synechocystis*, and myeloperoxidase (MPO). Furthermore, all available literature data about $E^{\circ\prime}$[Fe(III)/Fe(II)] values of chlorite dismutases are included: those from chlorite dismutases from *I. dechloratans* (IdCld), *D. aromatica* (DaCld), and *A. oryzae* (AoCld). Dashes indicate that no data are available.

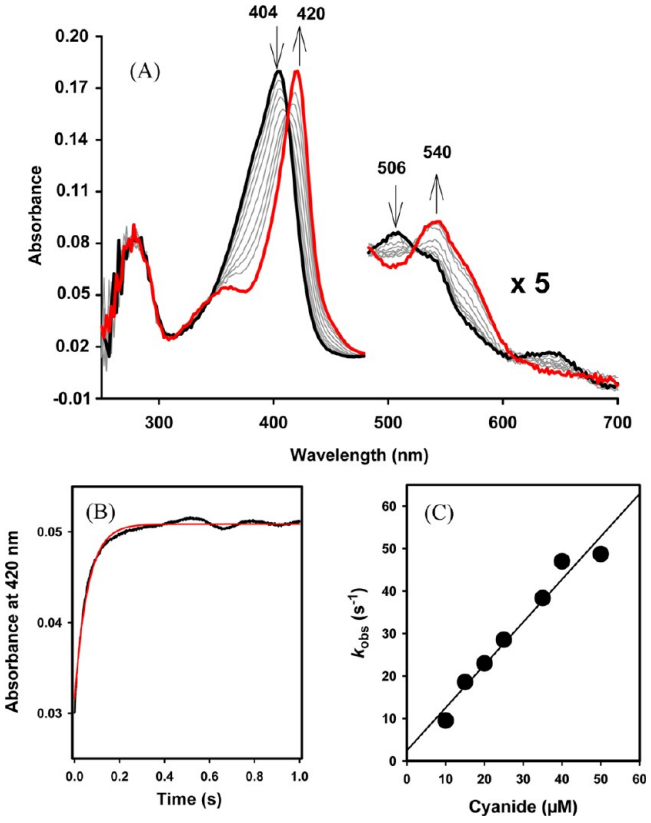

Figure 5. Transient-state kinetics of binding of cyanide to ferric chlorite dismutase from *N. winogradskyi* (NwCld). (A) Spectral changes upon reaction of 2 μM ferric NwCld with 10 μM cyanide measured in the conventional stopped-flow mode. The first spectrum is that of native NwCld; the second spectrum was recorded 1.3 ms after mixing, and subsequent spectra show the formation of the low-spin cyanide complex (absorbance maximum at 420 nm). Arrows indicate changes in absorbance with time. Conditions: 50 mM phosphate buffer, pH 7.0, and 25 °C. (B) Typical time trace at 420 nm with a single-exponential fit (1 μM NwCld and 15 μM cyanide). (C) Linear dependence of k_{obs} values from the cyanide concentration. The apparent association rate constant, k_{on}, was calculated from the slope and the apparent dissociation rate constant, k_{off}, from the intercept. The final concentration of NwCld was 1 μM in 50 mM phosphate buffer (pH 7.0).

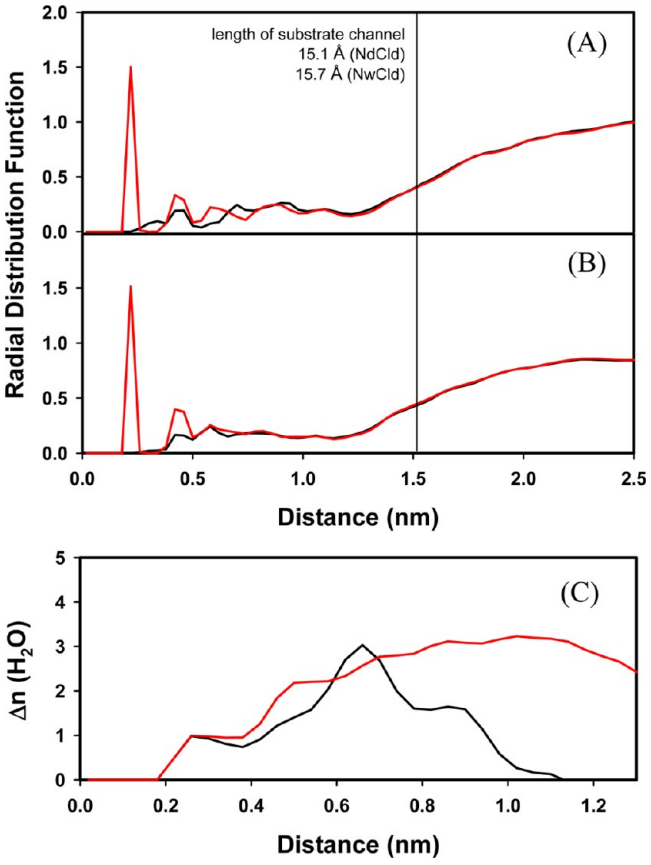

Figure 6. Radial distribution function of water molecules of high-spin ferric and ferrous chlorite dismutases from *Candidatus* "Nitrospira defluvii" (NdCld) and *N. winogradskyi* (NwCld). Radial distribution function with respect to the heme iron of NdCld (A) and NwCld (B) with oxidized states colored red and reduced states colored black. (C) Difference in the number of water molecules in the oxidized and reduced state, $\Delta n(H_2O)$, of NdCld (red) and NwCld (black).

It must be mentioned that $E^{\circ\prime}$ values of Clds from other sources reported so far (all available data are given in Table 3) range from −21 to −158 mV. Because the heme cavity architecture of all crystallized Clds[2−6] is almost superimposable (Figure 7B), this variability might result from different methods used in the determination of $E^{\circ\prime}$.[2,7,11,17] However, variability is also seen in the UV−vis spectra of those metalloproteins and in the kinetics of chlorite degradation. The ferric forms of chlorite dismutases from *I. dechloratans* (IdCld),[17] *D. aromatica* (DaCld),[11] and *A. oryzae* (AoCld)[2,7] (Table 3) were reported

dx.doi.org/10.1021/bi3013033 | *Biochemistry* 2012, 51, 9501−9512

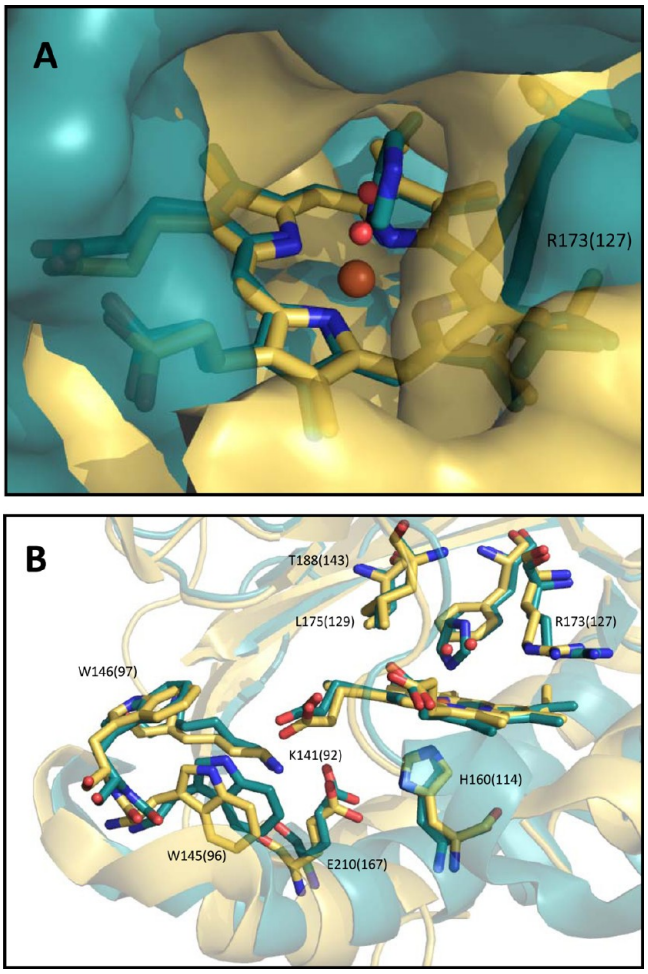

Figure 7. Structural analysis of the surface area at the substrate channel entrance and of the active site of chlorite dismutases from *Candidatus* "Nitrospira defluvii" (NdCld) and *N. winogradskyi* (NwCld). (A) Close-up of the surface area of substrate channels of NwCld (yellow, PDB entry 3QPI) and NdCld (cyan, PDB entry 3NN1). Catalytically active arginine 173(127) is highlighted. The crystal structure of NdCld shows an imidazole and that of NwCld two water molecules (red balls) bound to the distal heme side. (B) Superposition of active site residues of NwCld (yellow) and NdCld (cyan) and prosthetic groups. Amino acid numbering according to NdCld and NwCld (brackets). Figures were generated using PyMOL (http://www.pymol.org/).

to exhibit a rather broad Soret maximum around 392 nm, which is 13−16 nm blue-shifted compared to those of NwCld (405 nm) and NdCld (408 nm). At the same time, these enzymes show higher k_{cat} values of chlorite degradation compared to those of NdCld and NwCld, although comparison of kinetic parameters has been shown to be problematic because of the irreversible inhibition of the enzyme during chlorite degradation that starts to be relevant in different concentration regimes with different Clds.[5,10,11] On the other hand, chlorite dismutase from *Pseudomonas chloritidismutans* (PcCld)[35] exhibits a Soret absorbance of its resting state at 411 nm, similar to that of NdCld. Moreover, the related Dyp-type peroxidases, which together with chlorite dismutases constitute a distinct superfamily of heme enzymes because of similarities in overall fold and heme cavity architecture,[21] also exhibit Soret maxima in this range (404−409 nm).[36−41] Future comparative studies must be performed to elucidate the origin of the spectral differences among AoCld, DaCld, and IdCld on one hand as well as NdCld, NwCld, PcCld, and Dyp-type peroxidases on the other.

In addition to almost identical $E^{\circ\prime}$ values, the substrate access channels of NdCld and NwCld have similar lengths (15.1 and 15.7 Å, respectively) and bottleneck radii (2.8 and 2.6 Å, respectively). Moreover, the amount and distribution of water molecules in the ferric and ferrous state were shown to be very similar in the two metalloproteins (Figure 7A). This high degree of structural homology agrees with the overall chlorite degradation kinetics as well as the determined apparent bimolecular cyanide binding constants (2.6×10^6 and 1.0×10^6 M^{-1} s^{-1}, respectively) (Table 1).

When cyanide bound, the six-coordinate low-spin ($S = {}^1/_2$) forms of NdCld and NwCld were formed, inducing a significant decrease in the reduction potential of the Fe(III)/Fe(II) couple (−404 and −397 mV, respectively). The same phenomenon has been observed with other heme proteins.[17] Usually, in the ferrous high-spin form of heme proteins, the electrostatic interaction of the metal ion with the water molecules in the heme cavity is weakened compared to that in the ferric state.[22,42−45] This is also the case in Cld as has been demonstrated by the MD simulations of the ferric and ferrous forms of NdCld and NwCld (Figure 6). The electrostatic interaction described above is much smaller in the corresponding cyanide complexes, where the solvent accessibility to the heme is diminished.[22,42−45] As a consequence, the solvent-derived increase in entropy during the reduction reaction is significantly smaller in the six-coordinate low-spin cyanide adducts. In addition, the enthalpic stabilization of the ferric state is more pronounced and both phenomena lead to more negative $E^{\circ\prime}$ values (Table 2).[17,22,42−45]

To gain deeper insight into the mechanism of $E^{\circ\prime}$ modulation, the relative contributions of $\Delta H^{\circ\prime}_{rc}$ and $\Delta S^{\circ\prime}_{rc}$ were determined from $E^{\circ\prime}$ measurements at various temperatures (Table 3). The obtained values for both state functions (Table 3) were similar and demonstrated that the ferric state in native chlorite dismutases (NdCld and NwCld) is enthalpically stabilized (29 and 40 kJ mol^{-1}, respectively), whereas formation of the ferrous state is entropically favored (63 and 95 J mol^{-1} K^{-1}, respectively).

Reduction-induced changes in enthalpy and entropy contain contributions from both intrinsic protein-based factors ($\Delta H^{\circ\prime}_{rc,int}$ and $\Delta S^{\circ\prime}_{rc,int}$) and solvent-based factors ($\Delta H^{\circ\prime}_{rc,solv}$ and $\Delta S^{\circ\prime}_{rc,solv}$): $\Delta H^{\circ\prime}_{rc} = \Delta H^{\circ\prime}_{rc,int} + \Delta H^{\circ\prime}_{rc,solv}$, and $\Delta S^{\circ\prime}_{rc} = \Delta S^{\circ\prime}_{rc,int} + \Delta S^{\circ\prime}_{rc,solv}$.[17] It has been shown that $\Delta H^{\circ\prime}_{rc,int}$ is determined primarily by metal−ligand binding interactions and the electrostatics among the metal, the protein environment, and the solvent, whereas $\Delta S^{\circ\prime}_{rc}$ reflects the oxidation-state-dependent changes in conformational degrees of freedom of the polypeptide chain and solvent reorganization ($\Delta S^{\circ\prime}_{rc,solv}$) effects.[17] Our MD simulations have shown that the structures of both the protein and the prosthetic group in the Fe(III) and Fe(II) forms are very similar ($\Delta S^{\circ\prime}_{rc,int} \approx 0$), confirming that the change in entropy mainly reflects solvent reorganization ($\Delta S^{\circ\prime}_{rc} \approx \Delta S^{\circ\prime}_{rc,solv}$). This agrees with available data for the ferric and ferrous forms of other heme proteins that indicate that, in general, reduction-induced 3D structural changes are quite small in heme proteins.[17,42−45]

Because reduction-induced solvent reorganization effects usually induce compensatory enthalpy and entropy changes, the corresponding enthalpic contribution can be factored out from the measured enthalpy change,[17,44,46,47] finally allowing estimation of the protein-based contribution to $\Delta G^{\circ\prime}_{rc}$ =

dx.doi.org/10.1021/bi3013033 | *Biochemistry* 2012, 51, 9501−9512

$-nFE^{\circ\prime} = \Delta H^{\circ\prime}_{rc} - T\Delta S^{\circ\prime}_{rc} = \Delta H^{\circ\prime}_{rc,int} + \Delta H^{\circ\prime}_{rc,solv} - T\Delta S^{\circ\prime}_{rc,int} - T\Delta S^{\circ\prime}_{rc,solv}$. Because the solvent reorganization effects cancel exactly in the enthalpy and entropy, it follows that $\Delta G^{\circ\prime}_{rc} = -nFE^{\circ\prime} = \Delta H^{\circ\prime}_{rc,int} - T\Delta S^{\circ\prime}_{rc,int}$. Because the structures are very similar, the internal entropy change must be very small ($T\Delta S^{\circ\prime}_{rc,int} \approx 0$). Hence, to a first approximation, the measured $E^{\circ\prime}$ value coincides with $\Delta H^{\circ\prime}_{rc,int}$ and would ultimately be determined by the selective enthalpic stabilization of one of the two redox states by first coordination and electrostatic effects.[17,44,47] As a consequence, $\Delta H^{\circ\prime}_{rc,int} = -nFE^{\circ\prime}$ corresponds to 10.9 kJ/mol for NdCld and 11.5 kJ/mol for NwCld (Table 3). This approximation clearly suggests that in solution the heme iron environment in the two Clds is very similar.

In chlorite dismutases, the enthalpic stabilization of the ferric form could be attributed to the basic character of the proximal histidine (because of its hydrogen bond interaction with the nearby glutamate) (Figure 7B) and to the polarity of the distal heme site because of the presence of water molecules in the ferric state (Figure 6). In comparison with peroxidases that also have heme *b* as prosthetic group and a proximal histidine hydrogen-bonded to an acidic amino acid (i.e., aspartate) like HRP[39] or KatG[4] (Table 3), the polarity of the distal heme cavity is less pronounced because of the lack of the catalytic histidine. Recently, it has been reported that the imidazolate character of the proximal histidine in Cld is also less pronounced than in peroxidases because of weaker H-bonding interaction with the glutamate as suggested from recent resonance Raman spectroscopy measurements.[11,12] These differences could contribute to the more positive $E^{\circ\prime}$ values in Cld compared to those of most heme peroxidases, which (with the exception of MPO) have $E^{\circ\prime}$ values in the range from −180 to −320 mV (Tables 2 and 3).[17]

In summary, we could demonstrate that chlorite dismutases from both main lineages have, despite significantly different overall structures, a very similar active site and access channel architecture and as a consequence redox chemistry. Stabilization of the ferric high-spin state is important for efficient reaction with chlorite, thereby producing the enzyme intermediate Compound I and hypochlorite (reaction 1). Because within a defined heme enzyme the same molecular factors influence the redox properties of the heme iron at different oxidation states [e.g., in heme peroxidases, the hierarchy of $E^{\circ\prime}$ values of Fe(III)/Fe(II) couples reflects that of $E^{\circ\prime}$ values of the Compound I/ferric state couple],[17,47−51] it is reasonable to assume that the oxidation capacity of Cld Compound I is very high, possibly with $E^{\circ\prime}$ values of >1 V. This usually needs, to prevent unspecific oxidation of the protein matrix, stabilization of Compound I by (i) a partially (e.g., histidine H-bonded to Asp or Glu) or fully negatively charged (cysteinate or tyrosinate) proximal heme ligand and (ii) a short half-life of Compound I due to efficient reaction with the electron donor(s). In the case of Cld, both factors might contribute to partially prevent side reactions, although kinetic investigations have shown that with increasing chlorite concentrations the enzyme is progressively and irreversibly inactivated.[5−10]

■ ASSOCIATED CONTENT

Supporting Information

EPR simulation parameters of spectra from NdCld and NwCld (Table 1) and molecular dynamics simulations of NdCld and NwCld in the Fe(III) and Fe(II) states (Figure 1). This material is available free of charge via the Internet at http://pubs.acs.org.

■ AUTHOR INFORMATION

Corresponding Author

*Phone: +43-1-47654-6073. Fax: +43-1-47654-6050. E-mail: christian.obinger@boku.ac.at.

Funding

This project was supported by the Austrian Science Foundation, FWF [Doctoral program BioToP-Molecular Technology of Proteins (W1224) and FWF Project P25270-B22].

Notes

The authors declare no competing financial interest.

■ ACKNOWLEDGMENTS

We are grateful to Dr. Christopher W. M. Kay (University College London, London, U.K.), who provided the EPR spectrometer for low-temperature measurements.

■ ABBREVIATIONS

Cld, chlorite dismutase; NdCld, chlorite dismutase from *Candidatus* "Nitrospira defluvii"; NwCld, chlorite dismutase from *N. winogradskyi*; $E^{\circ\prime}$, standard reduction potential; $\Delta H^{\circ\prime}_{rc}$, enthalpy change for the reaction center upon reduction of the oxidized protein; $\Delta S^{\circ\prime}_{rc}$, entropy change for the reaction center upon reduction of the oxidized protein; SHE, standard hydrogen electrode; rdf, radial distribution function; rmsd, root-mean-square deviation; cw-EPR, continuous wave electron paramagnetic resonance; OTTLE, optical thin layer spectroelectrochemical; MD, molecular dynamics; PDB, Protein Data Bank.

■ REFERENCES

(1) Turano, P., and Lu, Y. (2001) Iron in heme and related proteins. In *Handbook of metalloproteins* (Bertini, I., Sigel, A., and Sigel, H., Eds.) pp 269−356, Marcel Dekker, Inc., New York.

(2) Ebihara, A., Okamoto, A., Kousumi, Y., Yamamoto, H., Masui, R., Ueyama, N., Yokoyama, S., and Kuramitsu, S. (2005) Structure-based functional identification of a novel heme-binding protein from *Thermus thermophilis* HB8. *J. Struct. Funct. Genomics 6*, 21−32.

(3) de Geus, D. C., Thomassen, E. A. J., Hagedoorn, P.-L., Pannu, N. S., van Duijn, E., and Abrahams, J. P. (2009) Crystal structure of chlorite dismutase, a detoxifying enzyme producing molecular oxygen. *J. Mol. Biol. 387*, 192−206.

(4) Goblirsch, B. R., Streit, B. R., DuBois, J. L., and Wilmot, C. M. (2010) Structural features promoting dioxygen production by *Dechloromonas aromatica* chlorite dismutase. *J. Biol. Inorg. Chem. 15*, 879−888.

(5) Kostan, J., Sjoeblom, B., Maixner, F., Mlynek, G., Furtmüller, P. G., Obinger, C., Wagner, M., Daims, H., and Djinovic-Carugo, K. (2010) Structural and functional analysis of the chlorite dismutase from the nitrite-oxidizing bacterium "*Candidatus* Nitrospira defluvii": Identification of a catalytically important amino acid residue. *J. Struct. Biol. 172*, 331−342.

(6) Mlynek, G., Sjöblom, B., Kostan, J., Füreder, S., Maixner, F., Gysel, K., Furtmüller, P. G., Obinger, C., Wagner, M., Daims, H., and Djinović-Carugo, K. (2011) Unexpected diversity of chlorite dismutases: A catalytically efficient dimeric enzyme from *Nitrobacter winogradskyi*. *J. Bacteriol. 193*, 2408−2417.

(7) van Ginkel, C. G., Rikken, G. B., Kroon, A. G. M., and Kengen, S. W. M. (1996) Purification and characterization of chlorite dismutase: A novel oxygen-generating enzyme. *Arch. Microbiol. 166*, 321−326.

(8) Hagedoorn, P. L., de Geus, D. C., and Hagen, W. R. (2002) Spectroscopic characterization and ligand-binding properties of

chlorite dismutase from the chlorate respiring bacterial strain GR-1. *Eur. J. Biochem. 269*, 4905−4911.
(9) Lee, A. Q., Streit, B. R., Zdilla, M. J., Abu-Omar, M. M., and DuBois, J. L. (2008) Mechanism of and exquisite selectivity for O-O bond formation by the heme dependent chlorite dismutase. *Proc. Natl. Acad. Sci. U.S.A. 105*, 15654−15659.
(10) Streit, B. R., and DuBois, J. L. (2008) Chemical and steady-state analysis of a heterologously expressed heme dependent chlorite dismutase. *Biochemistry 47*, 5271−5280.
(11) Streit, B. R., Blanc, B., Lukat-Rodgers, B. S., Rodgers, K. R., and DuBois, J. L. (2010) How active-site protonation state influences the reactivity and ligation of the heme in chlorite dismutase. *J. Am. Chem. Soc. 132*, 5711−5724.
(12) Blanc, B., Mayfield, J. A., McDonald, C. A., Lukat-Rodgers, G. S., Rodgers, K. R., and DuBois, J. L. (2012) Understanding how the distal environment directs reactivity in chlorite dismutase: Spectroscopy and reactivity of Arg183 mutants. *Biochemistry 51*, 1895−1910.
(13) Betley, T., Surendranath, Y., Childress, M., Alliger, G., and Fu, R. (2008) A ligand field chemistry of oxygen generation by the oxygen-evolving complex and synthetic active sites. *Philos. Trans. R. Soc. London, Ser. B 363*, 1293−1303.
(14) Poulos, T. L. (2010) Thirty years of heme peroxidase structural biology. *Arch. Biochem. Biophys. 500*, 3−12.
(15) Arnhold, J., Monzani, E., Furtmüller, P. G., Zederbauer, M., Casella, L., and Obinger, C. (2006) Kinetics and thermodynamics of halide and nitrite oxidation by heme peroxidases. *Eur. J. Inorg. Chem. 19*, 3801−3811.
(16) Furtmüller, P. G., Zederbauer, M., Jantschko, W., Helm, J., Bogner, M., Jakopitsch, C., and Obinger, C. (2006) Active site structure and catalytic mechanisms of human peroxidases. *Arch. Biochem. Biophys. 445*, 199−213.
(17) Battistuzzi, G., Bellei, M., Bortolotti, C. A., and Sola, M. (2010) Redox properties of heme peroxidases. *Arch. Biochem. Biophys. 500*, 21−36.
(18) Stenklo, K., Thorell, D., Bergius, H., Aasa, R., and Nilsson, T. (2001) Chlorite dismutase from *Ideonella dechloratans*. *J. Biol. Inorg. Chem. 6*, 601−607.
(19) Hofbauer, S., Gysel, K., Mlynek, G., Kostan, J., Hagmüller, A., Daims, A., Furtmüller, P. G., Djinovic-Carugo, K., and Obinger, C. (2012) Impact of subunit and oligomeric structure on the thermal and conformational stability of chlorite dismutases. *Biochim. Biophys. Acta 1824*, 1031−1038.
(20) Maixner, F., Wagner, M., Lücker, S., Pelletier, E., Schmitz-Esser, S., Hace, K., Spieck, E., Konrat, R., Le Paslier, D., and Daims, H. (2008) Environmenteal genomics reveals a functional chlorite dismutase in the nitrite-oxidizing bacterium "*Candidatus* Nitrospira defluvii". *Environ. Microbiol. 10*, 3043−3056.
(21) Goblirsch, B., Kurker, R. C., Streit, B. R., Wilmot, C. M., and DuBois, J. L. (2011) Chlorite dismutases, DyPs and EfeB: 3 microbial heme enzyme families comprise the CDE structural superfamily. *J. Mol. Biol. 408*, 379−398.
(22) Battistuzzi, G., Borsari, M., Ranieri, A., and Sola, M. (2002) Redox thermodynamics of the Fe(III)/Fe(II) couple in horseradish peroxidase and its cyanide complex. *J. Am. Chem. Soc. 124*, 26−27.
(23) Stoll, S., and Schweiger, A. (2006) EasySpin, a comprehensive software package for spectral simulation and analysis in EPR. *J. Magn. Reson. 178*, 42−55.
(24) Schmid, N., Christ, C. D., Christen, M., Eichenberger, A. P., and van Gunsteren, W. F. (2012) Architecture, implementation and parallelisation of the GROMOS software for biomolecular simulation. *Comput. Phys. Commun. 183*, 890−903.
(25) Schmid, N., Eichenberger, A. P., Choutko, A., Riniker, S., Winger, M., Mark, A. E., and van Gunsteren, W. F. (2011) Definition and testing of the GROMOS force-field versions 54A7 and 54B7. *Eur. Biophys. J. 40*, 843−856.
(26) Berendsen, H., Postma, J., Van Gunsteren, W., and Hermans, J. (1981) Interaction models for water in relation to protein hydration. In *Intermolecular Forces* (Pullman, B., Ed.) pp 331−342, D. Reidel Publishing Co., Dordrecht, The Netherlands.
(27) Berendsen, H., Postma, J., Van Gunsteren, W., DiNola, A., and Haak, J. (1984) Molecular dynamics with coupling to an external bath. *J. Chem. Phys. 81*, 3684−3690.
(28) Ryckaert, J., Ciccotti, G., and Berendsen, H. (1977) Numerical integration of the Cartesian equations of motion of a system with constraints: Molecular dynamics of n-alkanes. *J. Comput. Phys. 23*, 327−341.
(29) Berendsen, H., Gunsteren, W., Zwinderman, H., and Geurtsen, R. (1986) Simulations of Proteins in Water. *Ann. N.Y. Acad. Sci. 482*, 269−286.
(30) Tironi, I., Sperb, R., Smith, P., and van Gunsteren, W. (1995) A generalized reaction field method for molecular dynamics simulations. *J. Chem. Phys. 102*, 5451−5459.
(31) Heinz, T., van Gunsteren, W., and Hünenberger, P. (2001) Comparison of four methods to compute the dielectric permittivity of liquids from molecular dynamics simulations. *J. Chem. Phys. 115*, 1125−1136.
(32) Eichenberger, A. P., Allison, J. R., Dolenc, J., Geerke, D. P., Horta, B. A. C., Meier, K., Oostenbrink, C., Schmid, N., Steiner, D., Wang, D., and van Gunsteren, W. F. (2011) The GROMOS++ Software for the Analysis of Biomolecular Simulation Trajectories. *J. Chem. Theory Comput. 7*, 3379−3390.
(33) Petrek, M., Otyepka, M., Banás, P., Kosinová, P., Koca, J., and Damborský, J. (2006) CAVER: A new tool to explore routes from protein clefts, pockets and cavities. *BMC Bioinf. 7*, 316.
(34) Macedo, S., Pechlaner, M., Schmid, W., Weik, M., Sato, K., Dennison, C., and Djinović-Carugo, K. (2009) Can soaked-in scavengers protect metalloprotein active sites from reduction during data collection? *J. Synchrotron Radiat. 16*, 191−204.
(35) Mehboob, F., Wolterink, A. F., Vermeulen, A. J., Jiang, B., Hagedoorn, P. L., Stams, A. J., and Kengen, S. W. (2009) Purifcation and characterization of a chlorite dismutase from *Pseudomonas chloritidismutans*. *FEMS Microbiol. Lett. 293*, 115−121.
(36) Sugano, Y., Muramatsu, R., Ichiyanagi, A., Sato, T., and Shoda, M. (2007) DyP, a unique dye-decolorizing peroxidase, represents a novel heme peroxidase family: Asp171 replaces the distal histidine of classical peroxidases. *J. Biol. Chem. 282*, 36652−36658.
(37) Zubieta, C., Krishna, S. S., Kapoor, M., Kozbial, P., McMullan, D., Axelrod, H. L., Miller, M. D., Abdubek, P., Ambing, E., Astakhova, T., Carlton, D., Chiu, H. J., Clayton, T., Deller, M. C., Duan, L., Elsliger, M. A., Feuerhelm, J., Grzechnik, S. K., Hale, J., Hampton, E., Han, G. W., Jaroszewski, L., Jin, K. K., Klock, H. E., Knuth, M. W., Kumar, A., Marciano, D., Morse, A. T., Nigoghossian, E., Okach, L., Oommachen, S., Reyes, R., Rife, C. L., Schimmel, P., van den Bedem, H., Weekes, D., White, A., Xu, Q., Hodgson, K. O., Wooley, J., Deacon, A. M., Godzik, A., Lesley, S. A., and Wilson, I. A. (2007) Crystal structures of two novel dye-decolorizing peroxidases reveal a β-barrel fold with a conserved heme-binding motif. *Proteins 69*, 223−233.
(38) Ogola, H. J., Kamiike, T., Hashimoto, N., Ashida, H., Ishikawa, T., Shibata, H., and Sawa, Y. (2009) Molecular characterization of a novel peroxidase from the cyanobacterium *Anabaena sp.* strain PCC 7120. *Appl. Environ. Microbiol. 75*, 7509−7518.
(39) Roberts, J. N., Singh, R., Grigg, J. C., Murphy, M. E., Bugg, T. D., and Eltis, L. D. (2011) Molecular characterization of dye-decolorizing peroxidases from *Rhodococcus jostii* RHA1. *Biochemistry 50*, 5108−5119.
(40) van Bloois, E., Torres Pazmiño, D. E., Winter, R. T., and Fraaije, M. W. (2010) A robust and extracellular heme-containing peroxidase from *Thermobifida fusca* as prototype of a bacterial peroxidase superfamily. *Appl. Microbiol. Biotechnol. 86*, 1419−1430.
(41) Liers, C., Bobeth, C., Pecyna, M., Ullrich, R., and Hofrichter, M. (2010) DyP-like peroxidases of the jelly fungus *Auricularia auricula-judae* oxidize nonphenolic lignin model compounds and high-redox potential dyes. *Appl. Microbiol. Biotechnol. 85*, 1869−1879.
(42) Bellei, M., Jakopitsch, C., Battistuzzi, G., Sola, M., and Obinger, C. (2006) Redox thermodynamics of the ferric-ferrous couple of wild-type *Synechocystis* KatG and KatG(Y249F). *Biochemistry 45*, 4768−4774.

(43) Battistuzzi, G., Bellei, M., Zederbauer, M., Furtmüller, P. G., Sola, M., and Obinger, C. (2006) Redox thermodynamics of the Fe(III)/Fe(II) couple of human myeloperoxidase in its high-spin and low-spin forms. *Biochemistry 45*, 12750−12755.
(44) Battistuzzi, G., Bellei, M., De Rienzo, F., and Sola, M. (2006) Redox properties of the Fe^{3+}/Fe^{2+} couple in *Arthromyces ramosus* class II peroxidase and its cyanide adduct. *J. Biol. Inorg. Chem 11*, 586−592.
(45) Battistuzzi, G., Bellei, M., Borsari, M., Di Rocco, G., Ranieri, A., and Sola, M. (2005) Axial ligation and polypeptide matrix effects on the reduction potential of heme proteins probed on their cyanide adducts. *J. Biol. Inorg. Chem. 10*, 643−651.
(46) Battistuzzi, G., Bellei, M., Bortolotti, C. A., Rocco, G. D., Leonardi, A., and Sola, M. (2004) Characterization of the solution reactivity of a basic heme peroxidase from *Cucumis sativus*. *Arch. Biochem. Biophys. 423*, 317−331.
(47) Vlasits, J., Bellei, M., Jakopitsch, C., Furtmüller, P. G., Zamocky, M., Sola, M., Battistuzzi, G., and Obinger, C. (2010) Disruption of the H-bond network in the main access channel of catalase-peroxidase modulates enthalpy and entropy of Fe(III) reduction. *J. Inorg. Biochem. 104*, 648−656.
(48) Arnhold, J., Monzani, E., Furtmüller, P. G., Zederbauer, M., Casella, L., and Obinger, C. (2006) Kinetics and thermodynamics of halide and nitrite oxidation by heme peroxidases. *Eur. J. Inorg. Chem. 19*, 3801−3811.
(49) Jantschko, W., Furtmüller, P. G., Allegra, M., Livrea, M. A., Jakopitsch, C., Regelsberger, G., and Obinger, C. (2002) Redox intermediates of plant and mammalian peroxidases: A comparative transient-kinetic study of their reactivity toward indole derivatives. *Arch. Biochem. Biophys. 398*, 12−22.
(50) Furtmüller, P. G., Arnhold, J., Jantschko, W., Zederbauer, M., Jakopitsch, C., and Obinger, C. (2005) Standard reduction potentials of all couples of the peroxidase cycle of lactoperoxidase. *J. Inorg. Biochem. 99*, 1220−1229.
(51) Battistuzzi, G., Bellei, M., Vlasits, J., Banerjee, S., Furtmüller, P. G., Sola, M., and Obinger, C. (2010) Redox thermodynamics of lactoperoxidase and eosinophil peroxidase. *Arch. Biochem. Biophys. 494*, 72−77.